SUB-THz CHANNEL CHARACTERIZATION FROM RAY-BASED DETERMINISTIC SIMULATIONS

Grégory Gougeon, Yoann Corre, Mohammed Zahid Aslam
Infra Network Design (IND) department, SIRADEL, 2 Parc de Brocéliande, Saint-Grégoire, France

Abstract *– Future wireless communication systems will require large network capacities beyond the capabilities of present and upcoming 5G technology. The trend of considering higher frequencies for their large bandwidths continues today into the sub-THz domain. The frequencies that are considered in this article are the ones investigated in the BRAVE beyond-5G project, i.e. in the 90-200 GHz spectrum. A ray-based deterministic tool is extended to those frequencies, which are then exploited to simulate and characterize the propagation channel properties in two different scenarios: 1) in-office and 2) in-street. A particular interest is brought to the path loss and delay spread statistics. The impact of the antenna beam width is also considered. Using deterministic simulations (even if not yet validated in the target spectrum but at lower frequencies) is a very convenient way to explore the sub-THz propagation characteristics, while channel measurements are only very few at those frequencies. Some very simple models have been derived that may contribute to the elaboration and evaluation of future sub-THz systems.*

Keywords Channel modeling, ray-based model, sub-THz

1. INTRODUCTION

Many frequency bands in the so-called millimeter-wave spectrum (mmWave), between 10 and 90 GHz, are allocated today for fixed terrestrial communication radio links, and will be further exploited in 5G for mobile access or backhaul. Some interest of the telecommunication community that is preparing the next generation technologies is now moving to huge bandwidths available above 90 GHz. As pointed out in [1], up to 58.6 GHz bandwidth could be devoted to terrestrial communication services in spectrum between 90 and 200 GHz. Those frequencies, on which the present article is focusing, are either considered as part of the THz or sub-THz domain, depending on the interpretations. In the following, the term "sub-THz" is preferred.

The properties of the radio wave propagation in the 90-200 GHz band are not properly known, and no channel model (deterministic or stochastic) has been formally validated and recognized by the scientific community yet. The characteristics of the propagation channel and its modeling are nevertheless critical inputs for several research tasks: definition of adequate scenarios (cell range, supported propagation environments), elaboration of PHY-layer algorithms (e.g. waveform, channel estimation, equalization), evaluation and refinement of multi-antenna systems, link and system-level simulations.

The scientific propagation community is today producing intensive activity on the mmWave bands that are envisaged for 5G applications. These applications include a wide range of different solutions applied in backhauling, access, indoor and outdoor environments, large bandwidth and high antenna directivity scenarios. Recent channel models like WINNER+, METIS, mmMAGIC, MiWEBA or 3GPP offer solutions addressing frequencies above 6 GHz and often up to 100 GHz. The ITU also provides reference attenuation models up to 100 GHz (or beyond) for atmospheric gases, rain, vegetation and in-building penetration.

A sparse propagation channel is generally observed in mmWave bands, where the line-of-sight (LoS) direct path is the most dominant component. Many propagation paths that bring significant power at a lower frequency are either attenuated by obstacles or suffer from some interactions weakness (diffraction, diffuse scattering). That is still true in the sub-THz spectrum, and might even be slightly amplified. Nevertheless, some specular strong contributions are still present, leading to a few propagation clusters, along with significant delay and angular spreading. Main contributors are reflections on flat surfaces such as walls, floors or windows. Because the wavelength is lower than 3 mm, small objects, in particular metallic objects, may also cause a significant echo due to a reflection or scattering.

Remark that the channel sparsity is further increased by the use of highly-directive antennas, which will compensate for global higher path loss at mmWave or sub-THz frequencies. Some multi-paths transmitted and/or received out of the antennas beam width are filtered out. This effect has been captured by [2] where the 60-GHz delay and angular spreads do depend on the antenna beam width. Recommendations [2] and [3] propose a beam width-dependent model for different scenarios at 28 and 38 GHz in respectively indoor and outdoor environments.

Only a few scientific publications report today on channel characterization above 90 GHz. Channel sounding measurements, collected in a shopping mall at 28 and 140 GHz, are described and analyzed in [4]. Similar delay spreads and angular spreads are found in both frequency bands. Paper [5] reports on indoor measurements in bands V (60 GHz), E (70 – 80 GHz) and D (126 – 146 GHz). The delay spread is found to be lower in the D-Band. Even if similar propagation paths can be identified in each band, the longest echoes are not detected in the D-band (possibly due to limitation in the measured power dynamic). Paper [6] presents a large set of measurements in several bands up to 86 GHz with a focus on delay spread also. The conclusion is that delay spread does not vary much with frequency.

Two different scenarios are studied in the present article, radio propagation for in-office access and in-street backhaul. Section 2 describes the ray-based model that has been utilized to produce channel samples at various frequencies and situations, and how it has been upgraded. The simulation set-ups are detailed in section 3. The simulation results are reported in section 4, along with the analysis and the description of the derived path loss and delay-spread simplified models. Conclusions are summarized in section 5.

2. PROPAGATION CHALLENGES AND MODELING IN SUB-THZ BAND

The ray-based engine Volcano that is used to create the sub-THz prototype simulator has been successfully employed for more than 15 years in the sub-6 GHz band, and has already been utilized by the industry in the past few years in the mmWave domain up to 80 GHz [7]. Two different versions have been employed in the presented research: VolcanoFlex (devoted to small 3D environments) for the in-office predictions, and VolcanoUrban (optimized for large-scale outdoor areas) for the in-street predictions. Some evolutions have been required for this work, which are described in the two following subsections.

2.1 Extension of the EM material properties library up to 200 GHz

The original simulator relies on the definition of materials permittivity and conductivity frequencies up to 100 GHz, including those recommended by ITU [8, Table 3]. The current knowledge regarding the sub-THz materials properties is limited. Therefore, we decided to simply consider the ITU models at 100 GHz and extend their application up to 200 GHz. The correct implementation was validated by test simulations that assess the transmission, reflection and diffraction coefficients from the four following materials: glass, concrete, plasterboard and wood [9]. The plasterboard that is almost transparent below 6 GHz leads to more than 20 dB loss over most part of the sub-THz spectrum. Concrete walls are fully opaque above 60 GHz. Strong outdoor-indoor isolation, and room-to-room isolation in an indoor environment, are expected in sub-THz bands. Also reflection loss is observed constant with frequency while diffraction loss is higher. More precisely, the uniform theory of diffraction (UTD) loss remains the same at the optical frontiers, but rapidly degrades out of those frontiers. Additional degradation between 2 GHz and 200 GHz is found to be around 20 dB when considering a 90° concrete corner and incidence angle 45°.

2.2 Management of highly-detailed geographical representation

The VolcanoUrban tool [10] predicts several kinds of outdoor contribution, resulting from interactions with the building façades, the ground and the building rooftops. The ray-launching implementations allows for very fast computation of 3D multiple trajectories that combine reflections and diffractions, as well as propagation above rooftops. The losses due to the rooftop diffraction (or terrain diffraction) is computed from the well-known knife-edge diffraction technique, while the lateral building diffractions are calculated from UTD. The vegetation obstacles are managed specifically for frequencies above 6 GHz [11]. Both the transmission through the vegetation and the diffraction on bottom and top of the foliage are considered. The transmission is computed from an average linear loss (dB/m) that is multiplied by the

propagation length inside the foliage. The diffraction losses are given by the knife-edge approximation. The VolcanoUrban technology has recently been updated to support LiDAR point cloud data. This enables far more accurate 3D representation of the trees' foliage and street furniture compared to conventional geographical databases. Therefore, the prediction of the transmission losses and blockage is made much closer to reality [11].

3. SCENARIO AND SET-UP

The Volcano technology described in section 2 has been utilized in an indoor office scenario, and a street-level outdoor case study at sub-THz frequencies, details of which are described next.

3.1 In-office scenario

The considered environment is depicted in Fig. 1; it is a typical single-floor office of size 20 m x 10 m as described in [12]. It is composed of external walls, windows, internal walls, cubicle partitions (2 meters high) and desks. The propagation channel is computed from 10 different access points, which are installed at realistic locations i.e. on the wall or below the ceiling at 2.5 m height. 50 user locations at 1.5 m height are computed; they are distributed in the different rooms of the building. All the possible 500 links between the access points and the user locations are predicted, aiming at a statistical overview of the channel properties in this environment.

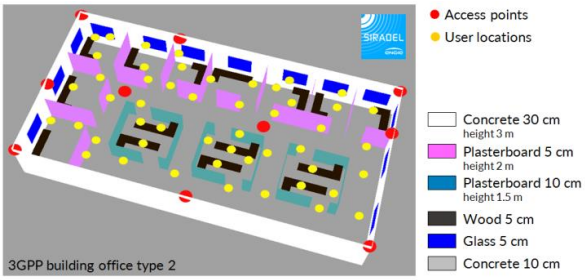

Fig. 1 – In-office scenario environment

The access points are considered with either isotropic, 6°-beam-width or 20°-beam-width antennas. These three simulations aim at comparing the channel properties as a function of the antenna beam width. The 20° and 6°-beam-width radiation patterns are representative of a beam-forming antenna system, which is foreseen to be mandatory in sub-THz communication in order to focus the energy towards the user, and thus benefit from better gain. In our study, the beam of the access point is automatically oriented towards the best propagation path (either direct or indirect). The user is equipped with an isotropic antenna in all three cases. The simulations are performed at various frequencies from 2 to 200 GHz in order to observe the channel evolution from medium cellular frequency bands to sub-THz bands.

3.2 In-street scenario

Prediction and characterization of the outdoor sub-THz propagation channel are conducted for urban fixed backhaul links at street level, typically for antennas installed at lamp-post height. LiDAR representation and ray-based multi-paths are together exploited to assess the impact of building and vegetation obstructions.

Point cloud LiDAR data was collected by SIRADEL in the centre of a North-American city (San Jose, USA). The modeled environment is composed of dense buildings with various heights (mostly greater than the simulated antenna heights). Trees are distributed along most of the streets. The study area may be considered as densely vegetated. The street poles, and lamp posts in particular, have been precisely classified as shown in Fig. 2.

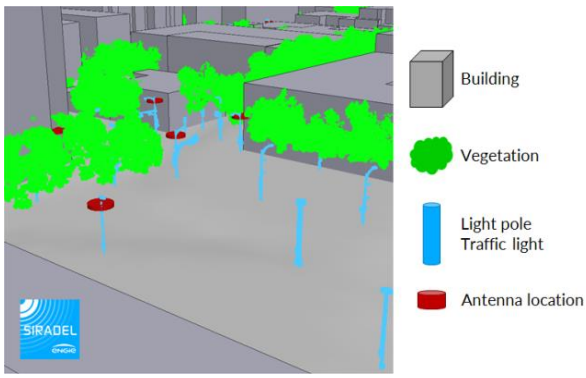

Fig. 2 – LiDAR representation

The lamp posts are considered as antenna positions of 8 meter height. All lamp-post-to-lamp-post possible links with a range lower than 200 meters are computed at frequency 150 GHz, leading to a total of 1873 predicted links.

Fig. 3 shows an example of received power variations predicted around one of the lamp posts (central point in the map). Considered EIRP is 30 dBm. Both transmit and receive antennas are highly directive and assumed to be aligned. The shadow effect behind trees and buildings can clearly be observed.

Instead of the traditional LoS/NLoS distinction, the links visibility distinguishes between LoS (line-of-sight), NLoS (building obstruction) and NloS-Vegetation (obstruction by only vegetation).

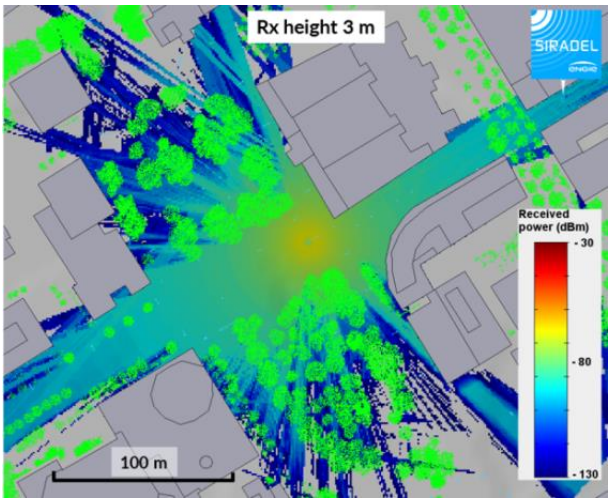

Fig. 3 – Outdoor received power map

The excess path loss (EPL) is computed as the difference between the free-space received power and the predicted power. It is found as a very convenient metric to observe and model how the environment impacts the propagation in this scenario.

Four antenna scenarios are considered: the three beam apertures described in the in-office scenario, but also an additional highly-directive case where only the strongest path (direct or indirect) is captured. As relevant in a fixed backhaul situation, the same antenna is assumed at both lamp post terminals. The vegetation linear loss (VLL) has a major impact on all predicted metrics. Three different values are considered, and compared: 6, 9 and 12 dB/m. The reasons are, first, that the vegetation losses vary with the kind of tree, and second, the vegetation impact has not yet been characterized at sub-THz frequencies. Note the simulated losses are far lower than the ones that could have been extrapolated from reference values in [13], but are in agreement with observations made by the authors at mmWave frequencies (tree VLL generally found much below 5 dB/m).

4. SIMULATION RESULTS

Simulation results, and derived models, are described for both the in-office and in-street scenarios.

4.1 In-office scenario

The 500 predicted path-loss values are approximated by a traditional model where the median path loss increases with log of distance:

$$PL = PLI + n \times 10\ log(d) + S \qquad (1)$$

The path loss PL is expressed in dB; n is the path-loss exponent; the distance d is expressed in meters; the path-loss intersect PLI, in dB, is the median loss at distance 1 meter; and S is a shadowing term in dB.

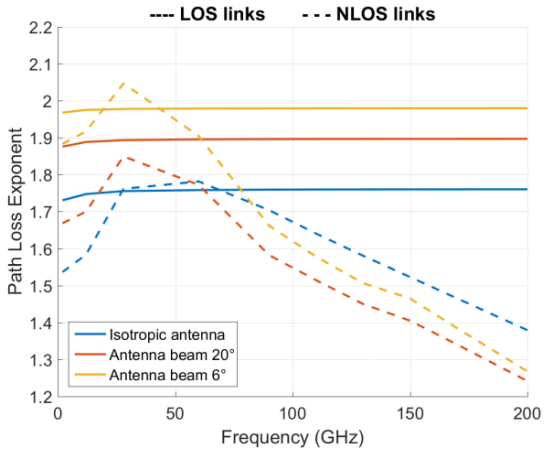

Fig. 4 – Path-loss exponent

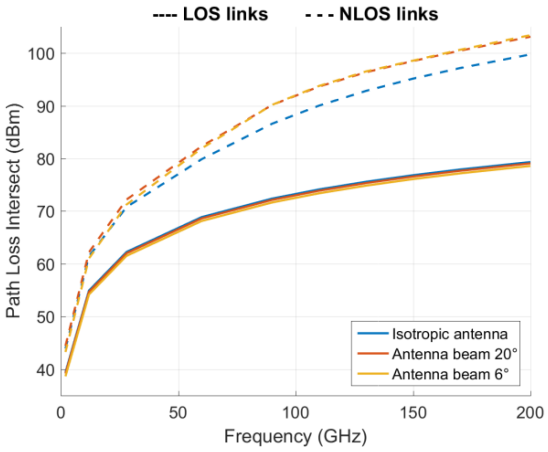

Fig. 5 – Path-loss intersect

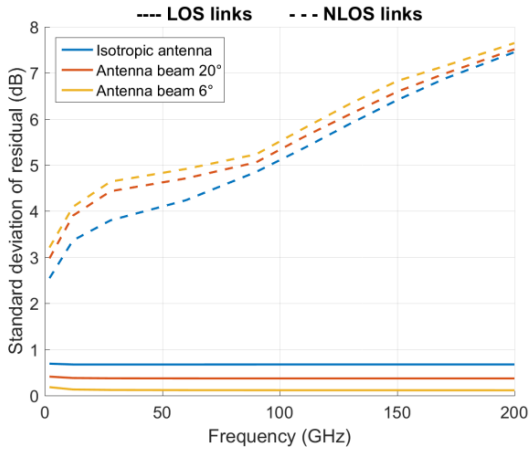

Fig. 6 – Standard deviation of the shadowing

The path-loss exponent n is calculated at various frequencies and for all considered antenna beam widths, as shown in Fig. 4. It is almost constant with frequency in LoS. The 6°-beam-width antenna

is acting as a filter that preserves the dominant direct path but removes most indirect paths, thus *n* is almost 2. With larger antenna beam width, the canyoning effect (or sum of multiple propagation paths caused by the strong reflections in this confined environment) leads to a received power greater or equal to the LoS direct path power; *n* is decreasing to 1.8. The NLoS path-loss exponent behaves very differently. At lower frequencies, as the transmission losses are weak, the obstructed direct path often remains the dominant path, the NLoS *n* value is quite similar to the ones observed in the LoS situation. But the multi-path effect becomes dominant at higher frequencies, especially above 28 GHz. As the main component in the received power comes from multiple non-obstructed reflected paths, *n* is rapidly decreasing, and finally reaches values below 1.5 at 150 GHz. But this is accompanied by a strong increase in the path-loss intersect (*PLI*), as shown in Fig. 5. The average difference between NLoS *PLI* at 60 GHz and 150 GHz is 16 dB while it is 8 dB in LoS. The remaining shadowing term *S* is characterized by its standard deviation, as plotted in Fig. 6. It is below 1 dB in the LoS situation, but rapidly increase with frequency in NLoS, in a quasi-linear way at the highest frequencies.

A simple sub-THz in-office path-loss model can be implemented as follows: the LoS probability is given as a function of distance; the median path loss is calculated from frequency-dependent n and PLI parameters; and the additional shadowing term S is considered as a log-normal variable with a frequency-dependent standard-deviation. The graphs given in Figures 4-6 are used to derive the approximate formulae shown in Table 1, valid in the range 90-200 GHz.

Table 1 – In-office path-loss simplified model (*d* is the distance in meters, and *f* is the frequency in GHz)

Acces point antenna	Isotropic	20°-beamwidth	6°-beamwidth
LoS probability (%)		$77 - 1.3 \times d$	
LoS Path-loss exponent PLE	1.76	1.90	1.98
LoS Path-loss intersect (dB)		$33 + 20 \times \log_{10}(f)$	
LoS shadowing std dev (dB)	0.7	0.4	0.1
NLoS Path-loss exponent PLE	$1.97 - 0.0029 \times f$	$1.85 - 0.0030 \times f$	$1.97 - 0.0035 \times f$
NLoS Path-loss intersect (dB)	$33 + 28 \times \log_{10}(f)$	$32 + 30 \times \log_{10}(f)$	$30 + 31 \times \log_{10}(f)$
NLoS shadowing std dev (dB)	$-10 + 3.3 \times \log_{10}(f)$	$-8.9 + 3.1 \times \log_{10}(f)$	$-8.5 + 3.1 \times \log_{10}(f)$

The effect of frequency and antenna directivity is also observed on the delay spread, considering a 30 dB power range in the channel response (weakest simulated paths are filtered out). The statistical distribution of the delay spread at 150 GHz is plotted in Fig. 7. In NLoS, the median isotropic delay spread is divided by 5 when applying a 20° beam, and divided by 19 with the narrower 6° beam. The reduction factor between the LoS istotropic and 20°-beam-width values is 4. Then the LoS median delay spread with 6° beam width goes to 0. The variation versus frequency is shown in Fig. 8. The LoS delay spread is almost constant with frequency, meaning the major indirect paths remain of the same relative magnitude at higher frequencies; they are caused by non-obstructed reflections. The NLoS delay spread tends to slowly decrease versus frequency when using a directive antenna (approaching 0 ns with the 6° beam). However the NLoS delay spread with isotropic antenna has a different behavior. It is growing from 2 to 100 GHz, as the direct path suffers from higher attenuation, but some delayed indirect paths remain strong.

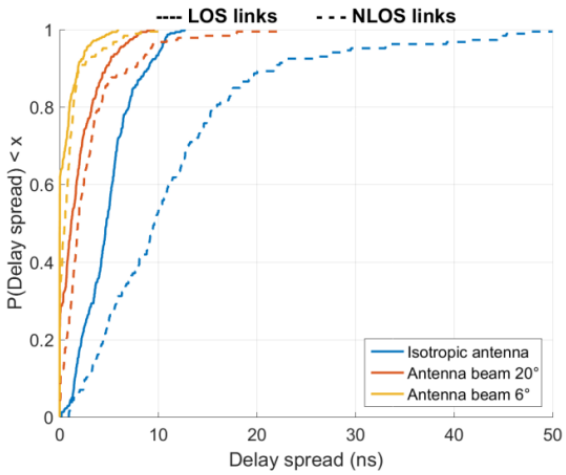

Fig. 7 – CDF of the delay spread at 150 GHz

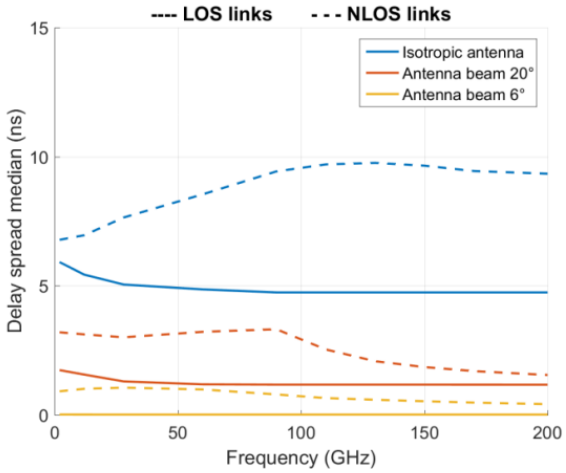

Fig. 8 – Median delay spread

A delay spread that increases with frequency does not match with common in-field observations. There are two main reasons. Firstly, the obtained results are specific to the semi-open confined area that has been simulated; secondly, measurements are generally affected by a factor that has not been

considered yet, i.e. the receiver sensitivity. In a practical system, some of the individual paths that are distinguished in low frequency bands may be received at a level inferior to the noise floor at a sub-THz frequency. The observed wideband characteristics of the measured channel depend on the receiver sensitivity or maximum allowed path loss (MAPL) at each considered frequency. Fig. 9 shows how the LoS and NLoS isotopric median delay spreads evolve with frequency, but this time, different MAPL constraints are considered.

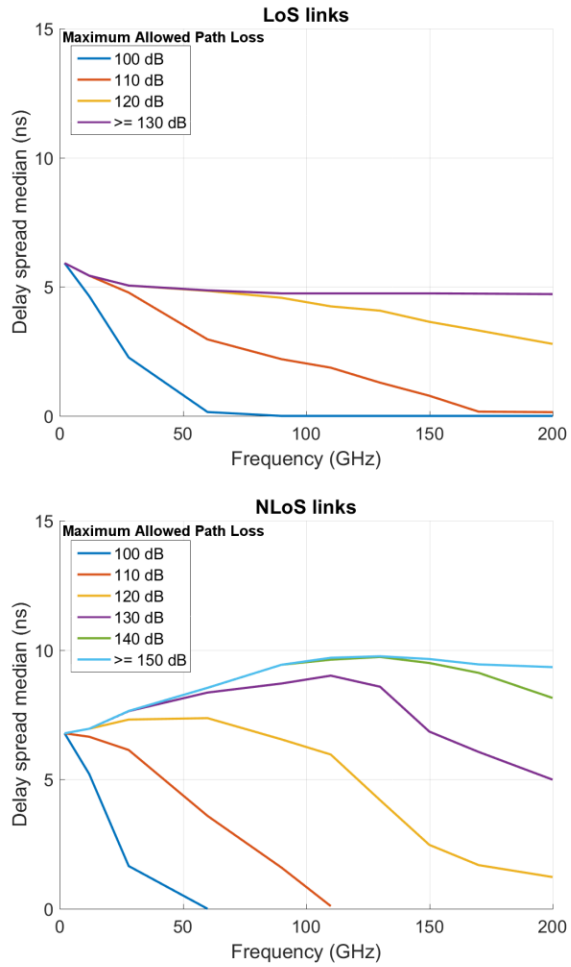

Fig. 9 – Median delay spread as a function of MAPL, for an isotropic antenna at the access point

The conclusion on the delay spread evolution significantly changes depending on the receiver sensitivity value. The NLoS median delay spread is observed as increasing with frequency when the receiver sensitivity is low, while it rapidly falls to only few ns in mmWave or sub-THz frequencies in case of a limited-performance receiver. The way the wideband channel properties are compared at different frequencies has to be done carefully. The delay spread may be strongly reduced in upper spectrum due to the receiver limitations but not directly to the propagation channel.

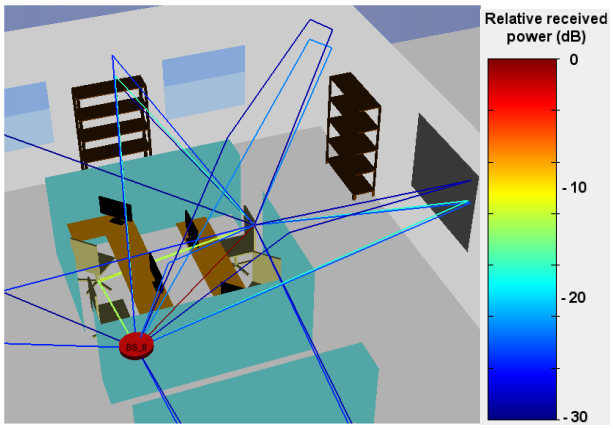

Fig. 10 – Propagation paths in office environment with furniture

The impact of furniture at 150 GHz has been studied by addition of shelves, boards, screens and chairs in the same office environment. Some of the links are subject to changes as shown in Fig. 10. But globally, as the user terminal is located above many of the added objects (1.5 m), the channel properties in terms of path loss, delay or angle statistics are not significantly modified. This would have to be further assessed with a lower terminal antenna.

4.2 In-street scenario

The propagation channel is predicted at 1873 lamp-post-to-lamp-post radio links in a North-American downtown area. The distribution between LoS, NLoS and NLoS-Vegetation is shown in Fig. 11 as a function of the distance. At the shortest ranges, the poles are mostly in LoS and NLoS-Vegetation situations, then NLoS occurrences rapidly increase and become the dominant configuration after 85 meters. At this distance, the LoS probability falls below 10%. The NLoS-Vegetation links are less than 20% at range 200 meters.

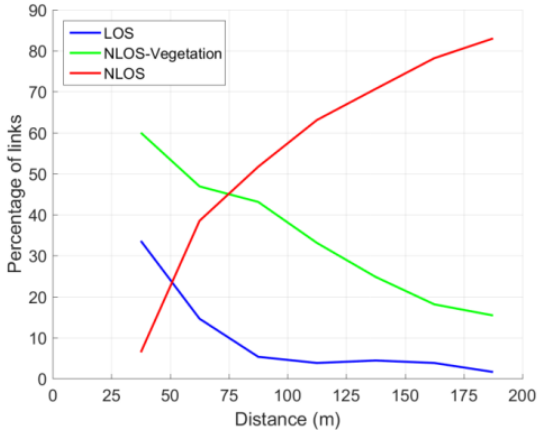

Fig. 11 – Visibility condition as a function of the distance

The CDF of the excess path loss (EPL) at 150 GHz is plotted in Fig. 12 for three different values of vegetation linear loss (VLL). The shown EPL is the one obtained with highly-directive antennas; however, the results are very similar with larger antenna beam widths. The NLoS EPL is about 50 dB higher than non-NLoS. It is hardly impacted by the VLL value, as the dominant propagation path is often due to rooftop diffraction, i.e. occurs above trees. The LoS percentage appears as the left CDF value in the plain curves: about 20%. The highest CDF values are associated to the NloS-Vegetation situation, where the VLL has a significant impact. As the foliage transmission is combined with foliage diffraction, the distance between EPL curves decreases when the VLL increases, i.e. when the diffracted path becomes dominant.

Fig. 13 shows the resulting EPL fitting functions for the different VLL values, and Fig. 14 shows the standard deviation of the residual path loss. This residual path loss is very high compared to general observations at lower frequencies (standard deviation lower or equal to 10 dB). It globally increases with distance.

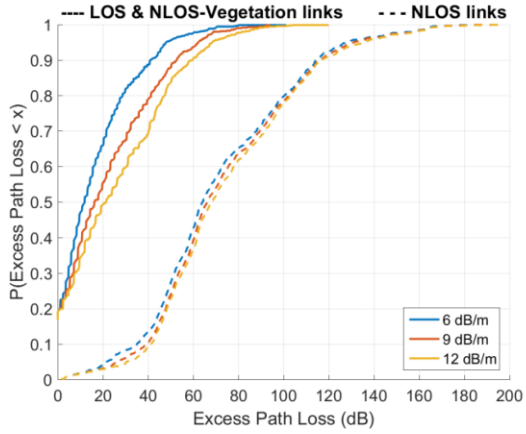

Fig. 12 – CDF of the excess path loss

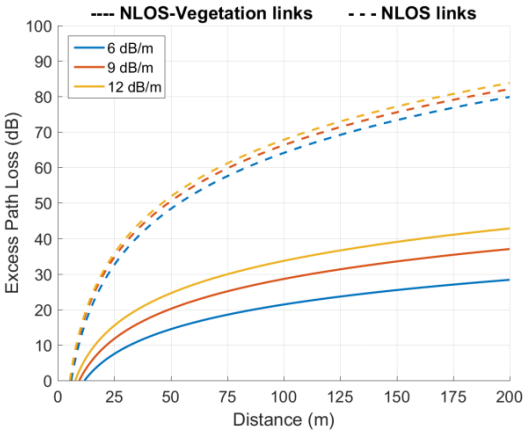

Fig. 13 – Excess path loss fit

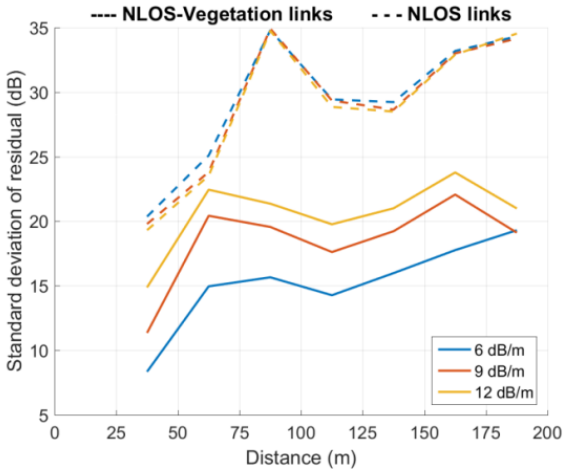

Fig. 14 – Standard deviation of the residual path loss

The highly-directive EPL can be approximated by a log-normal variable, where both the mean value and the standard deviation are log-distance dependent:

$$\mu\{EPL\} = A + B \times log(d) \qquad (2)$$

$$\sigma\{EPL\} = C + D \times log(d) \qquad (3)$$

The EPL parameters at 150 GHz are given in Table 2 for NLoS and NLoS-Vegetation situations (values are zero in LoS). Those values apply on distances greater than 25 up to 200 meters. They are proposed as a simplified model for the path loss experienced in urban street-level sub-THz fixed backhaul.

When considering different antenna beam widths, we observe only small changes in the EPL values, meaning the channel is dominated by a strong path. Actually, the delay spread is more significantly impacted. Fig. 15 shows how it is statistically distributed depending on the antenna beam width and visibility. The 90% quantile with the isotropic antenna is between 70 and 90 ns depending on the visibility condition. It is lower than 0.2 ns with the 6°-beam-width antenna. This is of particular importance in a backhaul system definition, where the performance and even the waveform can be affected by channel wideband properties, flat or selective. The vegetation scattering has not been predicted in this work; however, it may cause some spread in the delay domain even with a directive antenna, provided the dominant path crosses a tree.

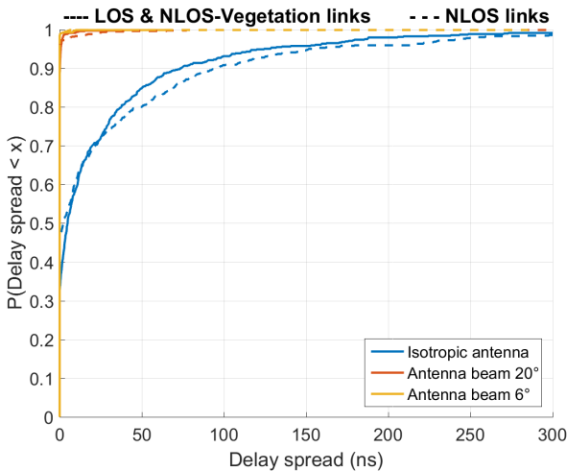

Fig. 15 – CDF of the delay spread

Table 2 – Excess path-loss parameters at frequency 150 GHz

	A (dB)		B (dB/dec)		C (dB)		D (dB/dec)	
VLL	NLoS-Veg	NLoS	NLoS-Veg	NLoS	NLoS-Veg	NLoS	NLoS-Veg	NLoS
6 dB/m	-24.8	-40.7	23.1	52.4	-10.2	-6.1	12.7	17.8
9 dB/m	-27.4	-38.7	28.0	52.5	-0.9	-8.2	9.7	18.7
12 dB/m	-26.9	-38.6	30.3	53.2	5.3	-10.1	7.6	19.5

5. CONCLUSION

The availability of large radio spectrum above 90 GHz offers opportunities to consider networks with immense capacities. Before such networks can be evaluated, it is important to validate the relevant scenarios and their requirements. Both indoor and outdoor scenarios at sub-THz frequencies have been considered in this work. Various propagation related properties like excess path loss and delay spread results have been reported for LoS, NLoS with vegetation and NLoS cases. Both isotropic and beam-forming antennas have been considered and reported.

This work enabled the extension of the existing channel modeling frameworks to be utilized for sub-THz frequencies. Detailed environmental data obtained from LIDAR point clouds was utilized to accurately consider the impact by various obstacles like vegetation. Extractions of analytical models from the channel characterization have also been performed to enable future utilization and validation by measurements of the sub-THz channels. The proposed simple sub-THz channel models can be further exploited to design, assess and evaluate the channels and networks until further specificities related to the channel are available through extensive measurements. In the meanwhile, this approach provides highly accurate initial understanding of the sub-THz channel.

ACKNOWLEDGEMENT

The research leading to these results received funding from the French National Research Agency (ANR-17-CE25-0013) within the framework of the project BRAVE. The authors are also grateful for the feedback obtained for this work in the framework of the COST Action CA15104 IRACON.

REFERENCES

[1] Y. Corre, G. Gougeon, J-B. Doré, S. Bicaïs, B. Miscopein, M. Saad, J. Palicot, F. Bader, and E. Faussurrier, "Sub-THz spectrum as Enabler for 6G Wireless Communications up to 1 Tbps", 6G wireless summit, Levi, Finland, March 2019

[2] ITU-R P.1238-9, *Propagation data and prediction methods for the planning of indoor radiocommunication systems and radio local area networks in the frequency range 300 MHz to 100 GHz*, June 2017.

[3] ITU-R P.1411-9, *Propagation data and prediction methods for the planning of short-range outdoor radiocommunication systems and radio local area networks in the frequency range 300 MHz to 100 GHz*, June 2017.

[4] S. Nguyen, J. Jarvelainen, A. Karttunen, K. Haneda and J. Putkonen, "Comparing Radio Propagation Channels Between 28 and 140 GHz Bands in a Shopping Mall", in the *Proc. of the 12th European Conf. on Antennas and Propagation (EuCAP)*, London, April 2018.

[5] L. Pometcu and R. D'Errico, "Characterization of sub-THz and mmWave Propagation Channel for Indoor Scenarios", in the *Proc. of the 12th European Conf. on Antennas and Propagation (EuCAP)*, London, April 2018.

[6] S. Nguyen et al., "On the Frequency Dependency of Radio Channel's Delay Spread: Analyses and Findings From mmMAGIC Multi-frequency Channel Sounding", in the *Proc. of the 12th European Conf. on Antennas and Propagation (EuCAP)*, London, April 2018.

[7] Y. Corre, T. Tenoux, J. Stéphan, F. Letourneux and Y. Lostanlen, "Analysis of Outdoor Propagation and Multi-Cell Coverage from Ray-Based Simulations in sub-6GHz and mmWave Bands", in the *Proc. of the 10th European Conf. on Antennas and Propagation (EuCAP)*, Davos, April 2016.

[8] ITU-R P2040-1, *Effects of building materials and structures on radiowave propagation above about 100 MHz*, July 2015.

[9] BRAVE, *Deliverable D2.0, Propagation channel model and RF impairments definition*, February 2019.

[10] Y. Corre and Y. Lostanlen, "Three-dimensional urban EM wave propagation model for radio network planning and optimization over large areas," *IEEE Transactions on Vehicular Technology*, 2009.

[11] J. Stephan, Y. Corre, R. Charbonnier and Y. Lostanlen, "Increased Reliability of Outdoor Millimeter-Wave Link Simulations by Leveraging Lidar Point Cloud", in the *Proc. of the 12th European Conf. on Antennas and Propagation (EuCAP)*, London, April 2018.

[12] P. Agyapong, V. Braun, M. Fallgren et al., ICT METIS, *Deliverable D6.1: simulation guidelines*, October 2013.

[13] ITU-R P.833-9, *Attenuation in vegetation*, September 2016.